6380–6392 *Nucleic Acids Research, 2014, Vol. 42, No. 10* *Published online 19 April 2014*
doi: 10.1093/nar/gku298

Requirement for Parp-1 and DNA ligases 1 or 3 but not of Xrcc1 in chromosomal translocation formation by backup end joining

Aashish Soni[1], Maria Siemann[1], Martha Grabos[1], Tamara Murmann[1], Gabriel E. Pantelias[2] and George Iliakis[1,*]

[1]Institute of Medical Radiation Biology, University of Duisburg-Essen Medical School, 45122 Essen, Germany and [2]Institute of Nuclear Technology and Radiation Protection, National Centre for Scientific Research "Demokritos," Aghia Paraskevi Attikis, 15310 Athens, Greece

Received November 29, 2013; Accepted March 29, 2014

ABSTRACT

In mammalian cells, ionizing radiation (IR)-induced DNA double-strand breaks (DSBs) are repaired in all phases of the cell cycle predominantly by classical, DNA-PK-dependent nonhomologous end joining (D-NHEJ). Homologous recombination repair (HRR) is functional during the S- and G2-phases, when a sister chromatid becomes available. An error-prone, alternative form of end joining, operating as backup (B-NHEJ) functions robustly throughout the cell cycle and particularly in the G2-phase and is thought to backup predominantly D-NHEJ. Parp-1, DNA-ligases 1 (Lig1) and 3 (Lig3), and Xrcc1 are implicated in B-NHEJ. Chromosome and chromatid translocations are manifestations of erroneous DSB repair and are crucial culprits in malignant transformation and IR-induced cell lethality. We analyzed shifts in translocation formation deriving from defects in D-NHEJ or HRR in cells irradiated in the G2-phase and identify B-NHEJ as the main DSB repair pathway backing up both of these defects at the cost of a large increase in translocation formation. Our results identify Parp-1 and Lig1 and 3 as factors involved in translocation formation and show that Xrcc1 reinforces the function of Lig3 in the process without being required for it. Finally, we demonstrate intriguing connections between B-NHEJ and DNA end resection in translocation formation and show that, as for D-NHEJ and HRR, the function of B-NHEJ facilitates the recovery from the G2-checkpoint. These observations advance our understanding of chromosome aberration formation and have implications for the mechanism of action of Parp inhibitors.

INTRODUCTION

Chromosomal translocations are a hallmark of cancer (1,2) and a key contributor to ionizing radiation (IR)-induced cell lethality (3). Double-strand breaks (DSBs) are precursor lesions for translocations and their formation implies error prone DSB processing. Higher eukaryotes have evolved several mechanisms for processing DSBs and for maintaining genomic stability. The two main pathways for DSB processing in higher eukaryotes are the classical, DNA-PK-dependent nonhomologous end joining (D-NHEJ) (frequently also termed classical or canonical C-NHEJ) (4–6), and homologous recombination repair (HRR) (7). An alternative end joining pathway is reported to become active when D-NHEJ (and as we show here also HRR) fails and is, therefore, considered to operate as backup, hence the term backup nonhomologous end joining (B-NHEJ) (8) (but frequently also called A-EJ).

Failure of D-NHEJ (or HRR) can be caused by a global loss of an essential factor through mutation in the encoding gene. However, D-NHEJ (or HRR) failures can also occur in a cell genetically proficient in D-NHEJ (or HRR) as a result of local failures in the processing of individual DSBs. Such local failures can be caused, for example, by errors during the assembly of the repair machinery, by local limitations in the availability of key factors, by the location of the DSB in the genome, by the compaction of neighboring chromatin or repair-unrelated compaction changes and last but not the least by the complexity of the DSB (9). B-NHEJ utilizes Parp-1 (10–12), DNA Ligase 3 (Lig3) and possibly its interacting partner Xrcc1 (10), as well as DNA Ligase 1 (Lig1) (13–15). Furthermore, Mre11 (16–18) and CtIP (19) are also implicated in this form of alternative end joining.

Information on the relative contribution of the above DSB repair pathways to the formation or suppression of translocations is of great importance for our understanding of genomic stability, the development of cancer and of IR-induced cell death. It is likely to also be useful in the design

*To whom correspondence should be addressed. Tel: +49 201 723 4152; Fax: +49 201 723 5966; Email: Georg.Iliakis@uk-essen.de

of advanced targeted therapies for the treatment of human cancer. The structural characteristics of leukemic translocation junctions indicate that key players in their formation are end joining events, mediated by one of the NHEJ repair pathways (5,20). Indeed, HRR does not seem to contribute to translocation formation (21,22).

While D-NHEJ is, in principle, capable of generating translocations, it appears to do so infrequently. Notably, D-NHEJ abrogation causes an increase in translocation formation suggesting that the pathway actually suppresses their formation (23–25). These observations leave B-NHEJ as the main culprit in translocation formation. In line with this expectation, Lig3 and CtIP contribute to chromosomal translocations generated by the error-prone processing of restriction endonuclease (RE)-generated DSBs (26,27). On the other hand, Xrcc1, the interacting partner of Lig3, appears dispensable for translocations forming during class switch recombination in B cells (28), although it is important for alternative end joining in a biochemical system (10). Although some of these reports provide hints on the mechanisms underpinning translocation formation after site-specific DSB induction, they do not address mechanisms underpinning translocations following miss-repair of stochastically induced DSBs and leave several questions unanswered regarding factors involved.

One key protein of B-NHEJ is Parp-1, thought to compete with Ku for DNA ends (29). Parp-1 has received special attention in recent years based on the clinical potential of its inhibitors, which exert synthetic lethality in tumors with defects in Brca1, Brca2 and other HRR proteins (30,31). Evidence for the involvement of Parp-1 in translocation formation is only now starting to emerge. Parp inhibitors reduce the frequency of translocations in G1 cells from site-directed DSBs, as well from DSBs induced by relatively high doses of IR (32). Whether Parp-1 contributes to translocation formation at lower doses of radiation and most importantly in other phases of the cell cycle remains unknown despite the potential relevance of the information to our mechanistic understanding of DSB processing in general and the consequences of Parp-1 inhibition in particular. Also, it remains unknown whether other components of B-NHEJ contribute to translocation formation, as well as whether interdependencies and interactions exist between B-NHEJ and checkpoint response, or between B-NHEJ and D-NHEJ or HRR.

Here, we investigate the mechanism of translocation formation and the contribution of B-NHEJ in this process using wild type (wt), as well as D-NHEJ- and HRR-deficient cells exposed during the G2-phase of the cell cycle to low, biologically and clinically relevant doses of IR (1 Gy). This is highly relevant to the mechanism of action of Parp-1 inhibitors in HRR-deficient cells, and important for understanding the response of tumors curatively treated with IR, which typically have growing cell fractions larger than the surrounding normal tissue and, thus, more G2-phase cells. Indeed, previous work shows that B-NHEJ activity is markedly increased in the G2-phase (33,34). We analyze shifts in translocation formation deriving from defects in D-NHEJ and/or HRR and identify B-NHEJ as the main repair pathway backing up both of these defects at the cost of a large increase in translocations formation. Our results clarify the function of Parp-1, Lig1, Lig3 and Xrcc1 in B-NHEJ, and demonstrate unanticipated connections between B-NHEJ DNA end resection and the G2-checkpoint. These observations advance our understanding of chromosome aberration formation and have implications for the mechanism of action of Parp inhibitors.

MATERIALS AND METHODS

Cell culture

All cell lines were incubated at 37°C in an atmosphere with 5% CO_2 and 95% air. Hamster cells, CHO10B4 wt and EM9 (Xrcc1m), were grown in minimum essential medium (MEM) supplemented with 10% fetal bovine serum (FBS) and antibiotics. MEFs (wt), *Lig4*$^{-/-}$, *Ku80*$^{-/-}$, *DNA-PKcs*$^{-/-}$, *Ku80*$^{-/-}$*DNA-PKcs*$^{-/-}$, *Rad54*$^{-/-}$ (347E), *Lig4*$^{-/-}$*Rad54*$^{-/-}$ (346B), *Lig1*$^{-/-}$ and *Parp1*$^{-/-}$ (35), were grown in Dulbecco's modified MEM supplemented with 10% FBS and antibiotics. Human colorectal tumor HCT116 cells, wt and *Lig4*$^{-/-}$, were grown in McCoy's 5A medium supplemented with 10% FBS and antibiotics.

Chemicals and inhibitors

Colcemid (L-6221, Biochrom AG) was used at 0.1 μg/ml to accumulate cells at metaphase (Stock: 10 μg/ml in phosphate-buffered saline (PBS) w/o Ca^{++}, Mg^{++}). Calyculin A (C-3987, LC laboratories) was used at a concentration of 50–100 nM (Stock: 10 μM in DMSO; dimethyl sulfoxide) for induction of premature chromosome condensation (PCC) during the G2-phase of the cell cycle. Carnoy's fixative was prepared by mixing 3 parts methanol (Sigma Aldrich) and 1 part glacial acetic acid (Carl Roth GmbH & Co.) just before use. A total of 2.5 ml of ready-to-use Giemsa stain (Carl Roth GmbH & Co.) was diluted in 50 ml of Sorenson's buffer (10582–013, Gibco, Invitrogen) to stain metaphase chromosomes, or PCCs. Entellan (Merck) was used as mounting medium.

The Parp-1 inhibitor PJ34 (Calbiochem) was used at 5 μM final concentration. 8-(4-Dibenzothienyl)-2-(4-morpholinyl)-4*H*-1-benzopyran-4-one (NU7441, Tocris), a DNA-PKcs inhibitor, was dissolved in DMSO at 10 mM and was used at 5 μM final concentration. L82 (Lig1 inhibitor) and L67 (Lig1 and Lig3 inhibitor) (36) were purchased from Specs (The Netherlands) and used at 100 μM final concentration. Mirin (sc-203144, Santa Cruz Biotechnology Inc., Chemistry Department of Indianapolis University) was used at 300 and 500 μM for translocation and DSB end resection assays, respectively.

Radiation exposure

Irradiations were carried out with an X-ray machine (GE-Healthcare) operated at 320 kV, 10 mA with a 1.65 mm Al filter (effective photon energy approximately 90 kV), at a distance of 50 cm and a dose rate of ∼1.3 Gy/min. Dosimetry was performed with a Physikalisch-Technische Werkstätten (PTW) and/or a chemical dosimeter, which were used to calibrate an infield ionization monitor. Cells were returned to the incubator immediately after exposure to IR.

Analysis of chromatid breaks (CBs) and chromatid or chromosome translocations

Exponentially growing cells were exposed to 1 Gy X-rays. Following irradiation cells were allowed to repair for 1–5 h at 37°C. Colcemid was added for 1 h to block cells just about to reach metaphase prior to harvesting the respective time point. For the 1 h time point, however, colcemid was added 30 min after IR (to allow division of cells at mitosis during irradiation) and was kept for only 30 min. Cells were trypsinized, treated in hypotonic solution (75 mM KCl) for 10 min at room temperature (RT) and fixed in Carnoy's fixative 3 times. Fixed cells were dropped on clean glass slides and stained with 3% Giemsa stain prepared in Sorenson's buffer. Standard criteria were used for scoring metaphases. Bright field microscopy (Olympus, Vanox-T, Japan) and a MetaSystems station (Altlussheim, Germany) with a microscope (AxioImager.Z2, Zeiss) and automated image capture and analysis capabilities were employed for scoring chromosome aberrations. During scoring and depending on the experiment, CBs and gaps (CBs), as well as chromatid or chromosome translocations were considered. The Ikaros software (Version 3.5, MetaSystems) was used to analyze images generated in the MetaSystems station. The protocol employed here for cytogenetic analysis in cells irradiated in G2 is a modification of a protocol that has been extensively used before for this purpose (37).

Premature chromosome condensation

To analyze chromosome damage prior to metaphase in cells still in interphase, exponentially growing cells were exposed to 1 or 5 Gy X-rays and allowed to repair at 37°C for 4 h. A total of 100 nM calyculin-A was subsequently added for 30 min to induce PCC before processing for cytogenetic analysis. The time of calyculin-A treatment is integrated in the calculation of the repair time. Cells with PCC were prepared as described for metaphase analysis. About 150 G2-PCCs from three independent experiments were scored.

Fluorescent *in situ* hybridization (FISH)

Exponentially growing cells were exposed to 2 Gy X-rays and collected by trypsinization 14 h post-IR. Colcemid was added 2 h before harvesting the cells. Samples were processed for cytogenetic analysis as described in the previous section. Two-chromosome FISH was performed using probes staining human chromosomes 1 and 2. Probes were purchased from MetaSystems and staining followed the instructions of the manufacturer. Slides were scanned using fluorescence microscopy in an automated analysis station controlled by the Metafer software (see above). Translocations were scored using the Isis software (Version 3.5, MetaSystems Germany).

G2-checkpoint analysis

Cells were harvested at various times after IR and fixed in 70% ethanol at –20°C. After fixation, cells were resuspended in 1 ml of 0.25% Triton X-100 in phosphate-buffered saline (PBST) and incubated on ice for 10 min. After centrifugation, the cell pellet was suspended in 500 μl of PBS containing 1% bovine serum albumin (BSA) and incubated at RT for 30 min. A polyclonal antibody specific for H3pS10 (Abcam, ab5176) was diluted 1:5000 in PBST and 150 μl was added to each sample and incubated for 1–1.5 h at RT. Cells were then washed with PBS and incubated with 100 μl of goat anti-rabbit AlexaFluor 488-conjugated antibody (Invitrogen) diluted 1:300 in PBST and incubated for 1 h at RT. After washing with PBS, cells were stained with propidium iodide (PI) and analyzed in a flow cytometer (Gallios, Beckman Coulter). Gating was applied to determine the proportion of cells positive for H3pS10, which represents the fraction of cells at metaphase, i.e. the mitotic index (MI). An alternative approach to study IR-induced G2-checkpoint is used by counting percentage of mitotic cells from Giemsa stained slides prepared for cytogenetic analysis (Figure 6). For this purpose, about 1500–2000 cells were counted for each sample under 10× magnification of bright field microscope and percentage of mitotic cells was calculated.

Indirect immunofluorescence

Poly(ADP)ribose (PAR) staining. Cells were grown on coverslips, rinsed with PBS and treated with or without 10 mM H_2O_2 in PBS at RT for 20 min. Rinsed coverslips were then incubated in prewarmed medium for 10 min at 37°C. Coverslips were rinsed in PBS and fixed with methanol–acetone (1:1, v/v) for 10 min at 4°C. Fixed cells were blocked in PBG (0.2% gelatine, 0.5% BSA fraction V in PBS) solution overnight at 4°C. Cells were incubated with a 1:200 diluted anti-PAR mouse monoclonal antibody (Alexis) for 1.5 h at RT. After washing with PBS, cells were incubated with an AlexaFluor488-conjugated secondary anti-mouse antibody for 1 h at RT. Cells were finally counterstained with 4',6-diamidino-2-phenylindole (DAPI) for 10 min at RT and mounted in Prolong-Antifade mounting media. Samples were scanned on a Leica TCS-SP5 confocal microscope. PAR staining was examined in *wt* and *Parp-1*$^{-/-}$ MEFs.

Flow cytometry-based RPA retention assay

Exponentially growing cells were irradiated with 10 Gy IR. Cells were trypsinized at 4 h post-IR. Suspended cells were permeabilized using 0.2% Triton in PBS for 2 min on ice, followed by fixation with 3% PFA–2% (Paraformaldehyde) sucrose and blocking in PBG (0.2% Gelatin and 0.5% BSA in PBS). After incubation with primary RPA mouse monoclonal antibody and Alexa488-conjugated mouse secondary antibody for 90 and 60 min, respectively, cells were washed and resuspended in PI with RNase A. Cells were analyzed by flow cytometry (Gallios, Beckman Coulter). G2 cells were identified by their DNA content assessed by PI staining and gated using Kaluza 1.2 (Beckman Coulter). The assay, as applied here (38), measures RPA accumulation to single-stranded DNA regions in G2 and is an indicator of DNA end resection at sites of DSBs.

Statistical analysis

Graphs were created in SigmaPlot 11.0. Statistical significance was determined using Student's *t*-test available in SigmaPlot 11.0. $*P < 0.05$, $**P < 0.01$, $***P < 0.001$, n.s. (not significant).

RESULTS

Defects in HRR and/or D-NHEJ markedly increase translocation formation in cells irradiated in G2-phase

To analyze repair or miss-repair events at the chromosome level in phases of the cell cycle where all DSB processing pathways (HRR, D-NHEJ and B-NHEJ) are active (mainly G2- and late S-phase), we adopted a previously developed cytogenetic protocol (37,39–43). In this protocol, cells are exposed to IR in different phases of the cell cycle as an asynchronous culture and analysis of chromosome damage is carried out when cells reach metaphase. Cell cycle-specific analysis is achieved by implementing a 1-h colcemid block to accumulate metaphases starting at different times after IR. Thus, when colcemid is added 1 h after IR, cells accumulating at metaphase during the 1 h of the block will represent cells that have been irradiated near the end of the G2-phase. Similarly, when colcemid is added 4 h after IR, cells accumulating at metaphase during the 1 h block will represent cells irradiated early in G2- or late in S-phase––assuming durations of 1 h for mitosis, 3 h for G2-phase and a short IR-induced G2-arrest. In the latter sample, cells reaching metaphase up to 4 h post-IR, when colcemid is absent, will divide and will thus be excluded from the analysis of metaphases at this time point. This experimental design is particularly attractive as it combines "high resolution" (1 h intervals analyzed) cell cycle-specific analysis with the power of cytogenetics and allows follow-up not only of repair, but also of miss-repair events at the chromosome level (Figure 1A).

With the above protocol, we investigated exponentially growing MEFs of different genetic background after exposure to IR (1 Gy) and scored specifically chromatid translocations for up to 4 h after IR. This time frame of analysis allows us to concentrate on events taking place in the G2-phase of the cell cycle. Figure 1A shows typical examples of translocations scored in this kind of experiment. Translocations are not detectable (n.d.) in wt cells analyzed 1 h after IR (Figure 1B). A modest increase in translocations is seen for cells analyzed 2 and 3 h after IR, and is followed by a decrease at 4 h. The absence of translocations at 1 h is suggestive of minimum time requirements for the formation of translocations in the wt genetic background and is discussed below.

Translocations observed in wt cells represent miss-joining events mediated either by D-NHEJ or B-NHEJ, as HRR is an unlikely candidate. Impairment in MEFs of D-NHEJ by deletion of *Lig4* causes a marked, time-independent increase in translocations (Figure 1B), again evident only after the 2-h time point. In line with previous observations (23–25), we conclude therefore that D-NHEJ suppresses the formation of IR-induced chromosome aberrations in G2 cells and implicate B-NHEJ in their formation. Considering that increase in translocations reflects the enhanced function of B-NHEJ when D-NHEJ is genetically compromised, the results also support the notion that B-NHEJ functions as backup to D-NHEJ, an aspect that we have extensively discussed in the past (9,44–46).

HRR is functional in G2. In an effort to characterize its role in translocation formation, we analyzed HRR-deficient

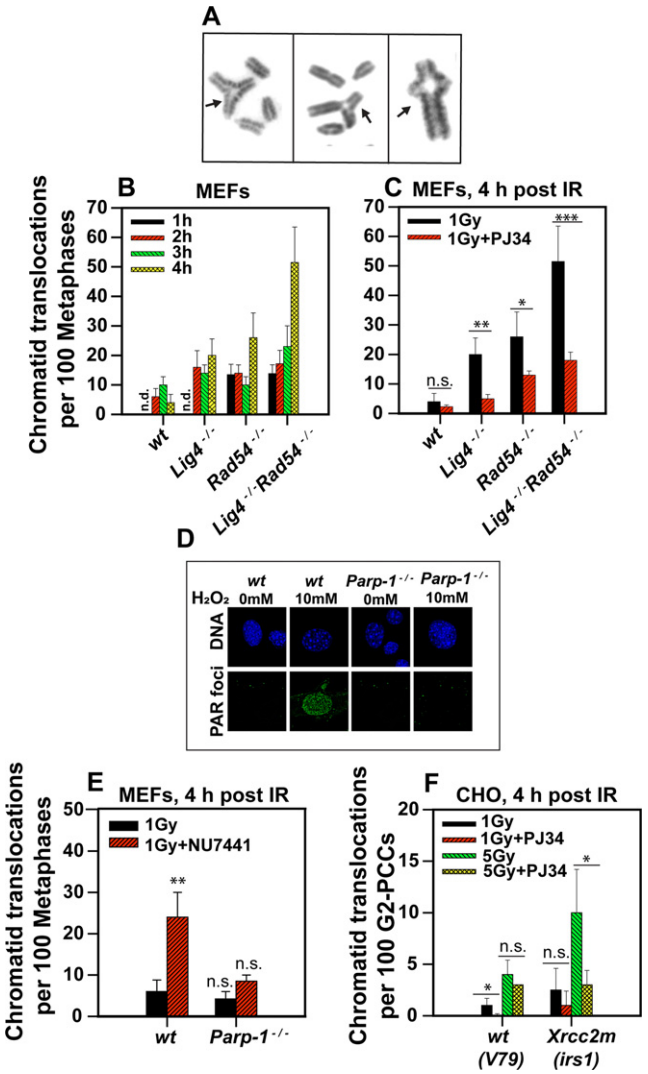

Figure 1. **(A)** Representative images of IR-induced chromatid translocations (indicated by arrows) as scored in the experiments described here. **(B)** Formation of translocations in wt, *Lig4*$^{-/-}$, *Rad54*$^{-/-}$ and *Lig4*$^{-/-}$*Rad54*$^{-/-}$ MEFs scored at metaphase 1–4 h after exposure to 1 Gy IR. A protocol specifically allowing the analysis of events occurring in the G2 of the cell cycle was employed (see text). Statistical analysis of observed differences among mutants is provided in Supplementary Table S1. The number of translocations per cell in nonirradiated controls were 0.0085 ± 0.01, 0.02 ± 0.03, 0.01 ± 0.0 and 0.02 ± 0.0 in wt, *Lig4*$^{-/-}$, *Rad54*$^{-/-}$ and *Lig4*$^{-/-}$*Rad54*$^{-/-}$ MEFs, respectively. **(C)** Effect of PJ34, a specific Parp inhibitor, on translocation formation in wt, *Lig4*$^{-/-}$, *Rad54*$^{-/-}$ and *Lig4*$^{-/-}$*Rad54*$^{-/-}$ MEFs analyzed at metaphase 4 h after exposure to 1 Gy IR. Statistical analysis of the results obtained and the differences among mutants is given in Supplementary Table S2. **(D)** Phenotype validation of *Parp-1*$^{-/-}$ MEFs through H_2O_2-induced PAR staining. Note that in the H_2O_2-treated cells, PAR staining is abundantly present in the wt, but completely absent in the knockout mutant. **(E)** Translocations in *wt* and *Parp-1*$^{-/-}$ MEFs scored 4 h after exposure to 1 Gy IR. Cells were incubated in the presence or absence of the DNA-PKcs inhibitor, NU7441, to inhibit D-NHEJ and facilitate B-NHEJ. Statistical analysis of the results is provided in Supplementary Table S3. **(F)** Translocation formation in prematurely condensed chromosomes (PCC) of G2-phase V79 (wt) and irs1 (*Xrcc2*m) Chinese hamster cells 4 h after exposure to 1 or 5 Gy of IR. Results obtained with samples incubated in the presence of PJ34 are also shown for comparison. All data in this figure represent the mean ± SD calculated from three independent experiments.

mutants. *Rad54*$^{-/-}$ MEFs show (Figure 1B) a marked increase in translocation formation, already notable at the 1-h time point. Translocations increase further and quite abruptly at the 4-h time point, likely coincident with the arrival at metaphase of cells irradiated late in S-phase or early in G2-phase. We conclude that similar to D-NHEJ, also HRR suppresses translocation formation during the G2-phase, and infer that HRR inactivation allows DSB processing by B-NHEJ at the price of translocation formation.

Thus, in the G2 phase of the cell cycle, B-NHEJ features as a universal backup, covering not only for D-NHEJ but also for HRR defects. The similar relative increase in translocations in D-NHEJ and HRR mutants suggests that at 1 Gy the contribution of HRR and D-NHEJ to this form of DSB repair is comparable. However, this conclusion is based on the unproven assumption that the inherent propensity for error-prone processing by B-NHEJ is for DSBs shunted from D-NHEJ defects similar to that of DSBs shunted from HRR defects. The increase in translocations observed already at the 1-h time point is unique to HRR defects. Results of an extensive, separate project suggest that it reflects altered cell-cycle progression and will be presented elsewhere.

To examine the independence or the interplay between D-NHEJ and HRR in the formation of translocations in G2, we also tested the double MEF mutant, *Lig4*$^{-/-}$*Rad54*$^{-/-}$. Surprisingly, the time points up to 3 h (Figure 1B) indicate only marginal increases in translocations compared to the single mutants. If this is not due to technical limitations of the assay, it will suggest that D-NHEJ and HRR are not operating independently in suppressing translocation formation within the period of examination. Dependencies may derive either from pathway interactions in the form of serial collaboration, or from operation, possibly in competition, in the prevention of the same miss-joining events. However, the result may also reflect the inability of B-NHEJ to efficiently cope with the entire load of DSBs in this highly repair deficient mutant. Notably, at the 4-h time point, we observe an abrupt increase in translocations, and an overall effect that reflects the sum of effects generated by D-NHEJ and HRR defects alone. Supplementary Table S1 summarizes the statistics of the results presented in Figure 1B and shows the statistical significance of the differences in translocation formation measured in the different mutants.

The majority of DSB miss-joining events underpinning translocations require Parp-1

To validate the role of B-NHEJ in translocation formation, we measured the contributions of putative associated factors. Parp-1 has been implicated in B-NHEJ due to its ability to bind DSBs and compete with Ku (29). Other studies suggest a role for Parp-1 in alternative pathways of end joining as well (10,12,47). To examine the involvement of Parp-1 in B-NHEJ events causing translocations, we carried out experiments similar to those described above, but in the presence of PJ34, a specific inhibitor of the Parp family of enzymes (48,49). We carried out scoring at the 4-h time point, where all mutants show the highest yields of translocations. The results summarized in Figure 1C show that PJ34 reduces by about half the incidence of translocations in wt and *Rad54*$^{-/-}$ cells, and by over two-thirds in *Lig4*$^{-/-}$ and *Lig4*$^{-/-}$*Rad54*$^{-/-}$ cells. The statistical analysis associated with the results in Figure 1C is given in Supplementary Table S2.

PJ34 targets several members of the Parp family (48,49). To specifically measure the contribution of Parp-1 in translocation formation, we examined *Parp-1*$^{-/-}$ MEFs (35). Figure 1D confirms the phenotype of the tested mutant by demonstrating complete loss of poly-ADP-ribosylation in response to H_2O_2 treatment, as compared to the wt control. Parp-1 deficient cells show reduced formation of translocations, compared to the wt, 4 h after exposure to 1 Gy X-rays, but this reduction fails to reach statistical significance. Inhibition of D-NHEJ in wt cells by NU7441, a DNA-PK inhibitor, allows DSB processing by B-NHEJ and causes, as expected, a marked increase in translocations. Notably, this increase is only marginal in the *Parp-1*$^{-/-}$ mutant. The reduction by two-thirds in translocation formation after NU7441 treatment in *Parp-1*$^{-/-}$ as compared to wt MEFs (Figure 1E) is similar to the reduction observed between *Lig4*$^{-/-}$ and the wt after treatment with PJ34 and demonstrates the critical and specific role of Parp-1 in the formation of translocations. The statistical analysis of the results associated with Figure 1E is given in Supplementary Table S3.

In all the above experiments, cells were analyzed for translocation formation at metaphase. Since it is likely that heavily damaged cells fail to reach metaphase at the time of examination, we used calyculin-A-mediated PCC, initiated 4 h after IR to examine translocation formation in G2. The results in Figure 1F show translocations in prematurely condensed chromosomes of wt V79 cells, which are almost completely eliminated by PJ34 after exposure to 1 Gy, and only slightly reduced after exposure to 5 Gy. In the HRR-deficient mutant, irs1 (defective in *Xrcc2*), translocation formation is increased compared to the wt at both doses tested and markedly reduced by PJ34. Thus, even in cells analyzed in G2 using PCC, translocation formation is strongly inhibited after inhibition of Parp-1.

The involvement of Parp-1 in translocation formation and the possible competition with Ku raise the question as to whether D-NHEJ mutants lacking Ku and/or DNA-PKcs show increased levels of translocations as compared to *Lig4*$^{-/-}$ MEFs. The results summarized in Figure 2A indicate that compared to wt or *Lig4*$^{-/-}$ MEFs, *Ku80*$^{-/-}$ MEFs analyzed in G2-phase have elevated yields of translocations. Notably, in Ku-deficient cells, translocations are already detectable at the 1-h time point. Increase in translocations, albeit to a smaller degree, is also observed in DNA-PKcs$^{-/-}$ MEFs and appears more pronounced in the double mutant, *Ku80*$^{-/-}$*DNA-PKcs*$^{-/-}$, as compared to either of the single mutants, although this increase fails to reach statistical significance (the statistical analysis of the results associated with Figure 2A is given in Supplementary Tables S4 and S5). In line with a strong involvement of Parp-1 in this process, treatment with PJ34 strongly inhibits translocation formation 4 h after IR in all mutants tested (Figure 2B and Supplementary Table S6).

To examine whether Parp-1 contributes to translocation formation not only in G2 but also in G1, we used a human

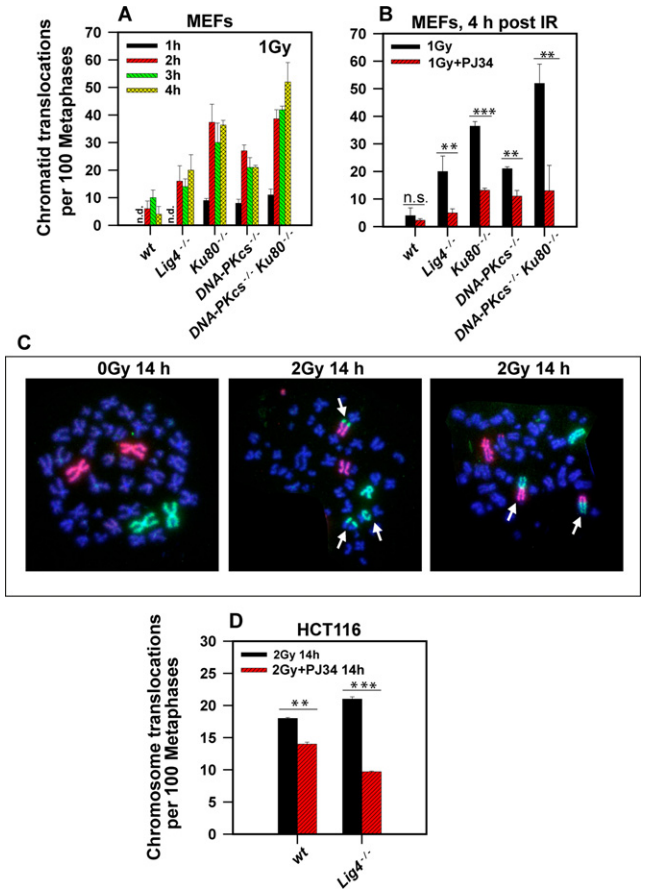

Figure 2. **(A)** Formation of translocations in wt, *Lig4*$^{-/-}$, *Ku80*$^{-/-}$, *DNA-PKcs*$^{-/-}$, *Ku80*$^{-/-}$ *DNA-PKcs*$^{-/-}$ MEFs, 1–4 h after exposure to 1 Gy IR. No translocations were detected in wt and *Lig4*$^{-/-}$ cells at 1 h post-IR. Statistical analysis and comparison of results obtained with the different mutants is provided in Supplementary Tables S4 and S5. **(B)** Translocation formation in wt, *Lig4*$^{-/-}$, *Ku80*$^{-/-}$, *DNA-PKcs*$^{-/-}$ and *Ku80*$^{-/-}$*DNA-PKcs*$^{-/-}$ MEFs 4 h after exposure to 1 Gy IR. Results obtained with samples subject to incubation with PJ34 are also shown. Statistical analysis and comparison of the results obtained in the different sets is given in Supplementary Table S6. **(C)** HCT116 metaphase spreads subject to FISH for chromosomes 1 (green) and 2 (red) and showing chromosome translocations (indicated by white arrows) generated by exposure to 2 Gy IR. **(D)** Effect of Parp-1 inhibition on the frequency of chromosome translocations in HCT116 wt and *Lig4*$^{-/-}$ cells, 14 h after exposure to 2 Gy IR. Statistical analysis and comparison between the results obtained is given in Supplementary Table S7. Data represent the mean ± SD from two to three independent experiments.

cell system to take advantage of a long G1-phase and opted for HCT116 cells for which D-NHEJ mutants are available (50). To detect translocations we used two-chromosome FISH and scored junctions between colored chromosomes 1 (green) and 2 (red), as well as between colored chromosomes and DAPI-stained chromosomes (blue). Figure 2C shows typical metaphases with chromosome-type translocations as scored in these experiments. In metaphases analyzed 14 h after IR, chromosome-type translocations are exclusively observed; this form of chromosome aberrations and the absence of chromatid-type translocations in the samples confirms that the causative events occurred in the G1-phase of the cell cycle.

While treatment with PJ34 only modestly reduces translocations in wt cells (Figure 2D), it reduces translocations by over a half in the *Lig4*$^{-/-}$-deficient HCT116 mutant (Figure 2D). This result demonstrates the involvement of Parp-1 in translocations forming in a human cell system in the G1-phase of the cell cycle, and shows that translocation formation is enhanced in D-NHEJ-deficient cells. The statistical analysis associated with the results in Figure 2D is given in Supplementary Table S7.

DNA ligases 1 and 3 contribute to the formation of translocations in G2-phase

Work using site-specific DSBs suggests a role of Lig1 and Lig3 in the formation of chromosome translocations (26). To examine this possibility for IR-induced random DSBs, we introduced two previously characterized DNA ligase inhibitors (36). L82 is reported to preferentially inhibit Lig1 and L67 to inhibit both Lig3 and Lig1. We tested the efficacy of these inhibitors in suppressing translocation formation in *Lig4*$^{-/-}$*Rad54*$^{-/-}$ MEFs since among all mutants they display the highest yields of translocations at 4 h after IR (Figure 1B). The results summarized in Figure 3A confirm the strong effect of PJ34 in this experimental setting. While inhibition of Lig1 by L82 confers no reduction in translocation formation, inhibition of both Lig1 and Lig3 by L67 generates a strong effect, similar to that observed with PJ34. Combination of L67 with PJ34 has no additional effect on translocation formation as compared to single inhibitor treatment suggesting that Parp-1 and the DNA ligases 1 and 3 operate on the same subset of DSBs (Figure 3A). We conclude, in line with published data that B-NHEJ utilizes preferentially Lig3, and possibly also Lig1 when Lig3 is inhibited or absent (see also below). The statistical analysis associated with the results in Figure 3A is given in Supplementary Table S8.

Xrcc1 is dispensable for the formation of IR-induced translocations, but it reinforces the competitive advantage of Lig3

The involvement of Lig3 in B-NHEJ-mediated formation of translocations implies a requirement for its cofactor, XRCC1. To address this question we tested a CHO mutant, EM9, defective in the gene coding for this protein. Compared to the wt CHO, EM9 cells show similar induction of translocations at metaphase, 4 h after 1 Gy of IR (Figure 3B). Inhibition of D-NHEJ by NU7441 causes the expected increase in translocations in CHO cells. Notably, a similar increase in translocations is also observed in EM9 cells despite the defect in Xrcc1. Formation of translocations in EM9 cells remains sensitive to Parp-1 inhibition as indicated by their reduction after treatment with PJ34 (Figure 3B).

An interpretation for the results shown in Figure 3B is that in the absence of Xrcc1, Lig3 is completely inactivated and translocation formation is exclusively catalyzed by Lig1. Alternatively, it is possible that Lig3 remains functional in the absence of Xrcc1 and contributes, possibly together with Lig1, to translocation formation. To test these alternatives, we measured translocation formation in wt CHO and EM9 cells after exposure to 1 Gy X-rays and

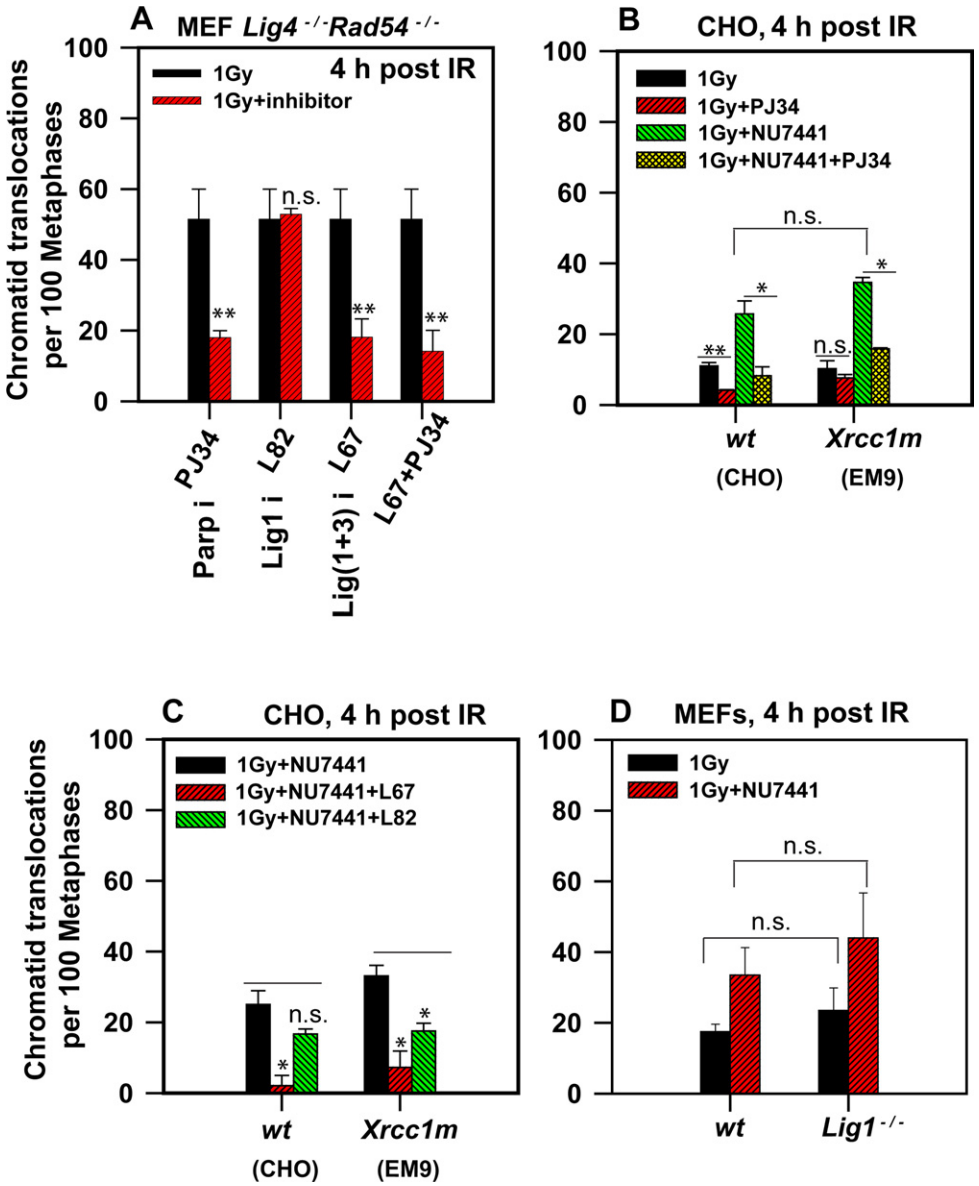

Figure 3. **(A)** Effect of inhibition of DNA ligases on translocation formation in *Lig4*$^{-/-}$*Rad54*$^{-/-}$ MEFs, as measured 4 h after exposure to 1 Gy IR. The inhibitors L82, L67 and a combination of PJ34 with L67 were administered 1 h prior to IR. The identity of the DNA ligases inhibited by each of these compounds is shown in the figure. Statistical analysis and intercomparison of the results obtained is provided in Supplementary Table S8. **(B)** Translocation formation in CHO (wt) and EM9 (Xrcc1 mutant) cells as measured at metaphase 4 h after exposure to 1 Gy IR. Results obtained with cultures exposed to PJ34 and NU7441 are also shown. **(C)** Effect of inhibition of DNA ligases 1 and 3 on translocations formation in CHO and EM9, as measured 4 h after exposure to 1 Gy IR. **(D)** Translocation formation in *wt* and *Lig1*$^{-/-}$ MEFs scored 4 h after exposure to 1 Gy IR. Cells were incubated in the presence or absence of the DNA-PKcs inhibitor, NU7441. Data represent the mean ± SD from two or three independent experiments.

treatment with NU7441 (to emphasize B-NHEJ function) in the presence or absence of the Lig1 inhibitor, L82 and Lig (1+3) inhibitor, L67. The results are summarized in Figure 3C.

In CHO cells treatment with L82 causes a small and not statistically significant decrease in translocation formation pointing again to only a small contribution of Lig1 when Lig3 together with Xrcc1 are present. In contrast, treatment with L67, that inhibits both Lig3 and Lig1, causes a pronounced decrease in translocation formation confirming the strong contribution of Lig3 in the process. In EM9 cells, treatment with L82 causes a statistically significant decrease in translocation formation indicating that in the absence of Xrcc1 Lig1 gains ground in translocation formation. However, treatment with L67 reduces even further translocation formation indicating that Lig3 remains at least partly active in the absence of Xrcc1. Thus, Xrcc1 is not absolutely required for the function of Lig3 in translocation formation, but underpins the competitive advantage of Lig3 against Lig1 frequently observed in the results summarized above.

To investigate further the role of Lig1, we measured translocation formation in wt and *Lig1*$^{-/-}$ MEFs after exposure to 1 Gy X-rays and treatment with NU7441 (Figure 3D). Translocation formation is similar in wt and

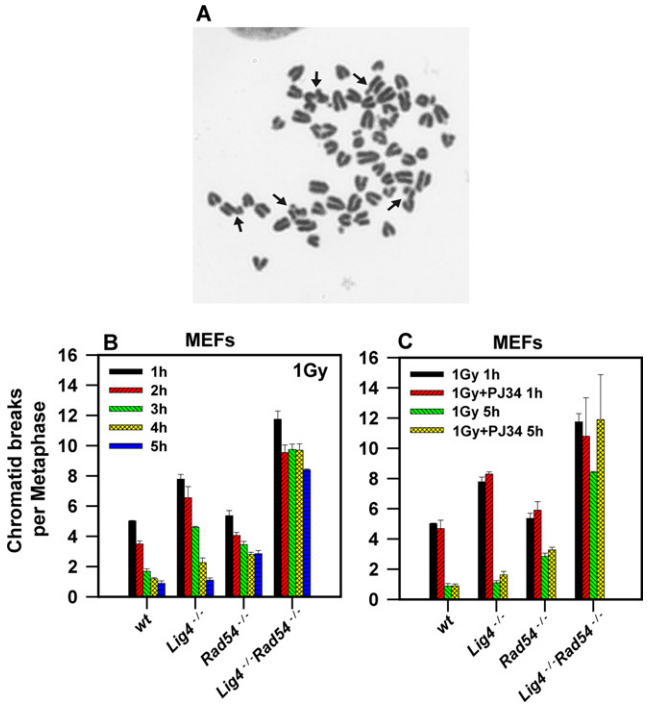

Figure 4. **(A)** Metaphase spread of a wt MEF at 1 h after exposure to 1 Gy IR showing CBs (indicated by arrows). **(B)** Kinetics of CB repair in wt, *Lig4*$^{-/-}$, *Rad54*$^{-/-}$ and *Lig4*$^{-/-}$*Rad54*$^{-/-}$ MEFs, as measured 1–4 h after exposure to 1 Gy IR. The number of CBs per cell in 0 Gy controls were 0.14 ± 0.15, 0.063 ± 0.03, 0.04 ± 0.01 and 0.1 ± 0.05 in wt, *Lig4*$^{-/-}$, *Rad54*$^{-/-}$ and *Lig4*$^{-/-}$*Rad54*$^{-/-}$ MEFs, respectively. Statistical analysis and intercomparison of the results obtained is provided in Supplementary Table S9. **(C)** Effect of Parp inhibition on CB repair as measured in wt, *Lig4*$^{-/-}$, *Rad54*$^{-/-}$ and *Lig4*$^{-/-}$*Rad54*$^{-/-}$ MEFs, 1 or 5 h after exposure to 1 Gy IR. Statistical analysis and intercomparison of the results obtained is provided in Supplementary Table S10. Data represent the mean ± SD from three independent experiments.

Lig1$^{-/-}$ MEFs confirming again that Lig1 is not contributing to translocation formation in the presence of the other DNA ligases.

Collectively, the above observations suggest that both Lig1 and Lig3 can catalyze the ligation events underlying translocation formation. Lig3 can function in translocation formation even in the absence of Xrcc1. However, in the absence of Xrcc1, Lig3 loses its competitive advantage against Lig1 and makes a smaller contribution to the overall effect. Notably, even in the absence of Xrcc1, translocation formation remains partly sensitive to Parp inhibition suggesting that in this function integration of Parp-1 and Lig3 activities through interaction with Xrcc1 is not required.

Defects in D-NHEJ and/or HRR have much smaller effect on CB repair than in translocation formation

The above analysis was focused on the formation of translocations in cells irradiated in the G2-phase of the cell cycle. Yet, the experimental protocol employed also allows analysis of CB repair in G2 cells. Figure 4 summarizes results obtained by scoring CBs as a function of time after IR. Figure 4A shows a representative metaphase with distinct CBs. In Figure 4B, the first set of data shows the development of CBs in wt cells analyzed 1–5 h after IR. The rapid reduction in the number of CBs is indicative of DSB processing by all DSB repair pathways. Over 80% repair is observed 5 h after IR. This kinetics is only slightly delayed when D-NHEJ is compromised by knocking out Lig4. A strong delay in chromatid repair is observed after impairment of HRR through *Rad54* deletion and this impairment is further exacerbated in the double mutant, *Lig4*$^{-/-}$*Rad54*$^{-/-}$. Considering that translocation formation is highest in this double HRR and D-NHEJ mutant, we conclude that B-NHEJ shows processing preference to DSBs destined to form exchanges. On the other hand, miss-joining events leading to chromosome exchange formation are likely to benefit from the persistence of CBs in cells deficient in HRR and D-NHEJ. The statistical analysis associated with the results in Figure 4B is given in Supplementary Table S9.

Notably, inhibition of Parp-1 has a much smaller effect on CB repair than in the formation of translocations suggesting again different processing mechanisms or quantitative differences in the participating DSBs (Figure 4C and Supplementary Table S10). This observation is in line with the modest effect of Parp-1 inhibition on the repair of DSBs induced by high doses of IR when analyzed by pulsed-field gel electrophoresis (29). Thus, while translocation formation in D-NHEJ- and/or HRR-deficient cells relies heavily on Parp-1, in the same cells, CB and DSB repair can be efficiently mediated by Parp-1-independent mechanisms.

Crosstalk between B-NHEJ and the G2-checkpoint

We used Parp-1 inhibition as a tool to investigate the possible crosstalk between B-NHEJ and the G2-checkpoint. For this purpose, we measured the MI using histone H3pS10 immunostaining combined with flow cytometry, as a function of time after IR in MEFs of different genetic background. Figure 5A illustrates MI estimation in *Lig4*$^{-/-}$ MEFs at 0, 1 and 5 h following exposure to 1 Gy IR.

In wt MEFs inhibition of Parp-1 prolongs G2 arrest (Figure 5B) suggesting that a considerable fraction of DSBs is processed, or signaled from, in a Parp-1-dependent and thus possibly also B-NHEJ-dependent manner. A very strong and persistent reduction in MI is observed after 1 Gy of IR in *Lig4*$^{-/-}$ and *Rad54*$^{-/-}$ MEFs indicative of a large enhancement of the G2-checkpoint response from defects in D-NHEJ or HRR. Inhibition of Parp-1 in these mutants causes no further potentiation in the checkpoint response (Figure 5C and D, respectively). Notably, however, a strong potentiation of the G2-checkpoint is observed in the double mutant, *Lig4*$^{-/-}$ *Rad54*$^{-/-}$, after treatment with PJ34, where B-NHEJ is the only active DSB repair pathway (Figure 5E). Thus, Parp inhibition uncovers a marked contribution of B-NHEJ to the recovery of cells from the G2-checkpoint.

We inquired whether inhibition of DNA ligases produces effects on the G2-checkpoint equivalent to those measured after treatment with the Parp inhibitor. In Figure 6A, the first set of data confirms the activation of the G2-checkpoint at 1 h and its complete recovery after 4 h in CHO cells exposed to 1 Gy X-rays. The right set of data in Figure 6A shows that this recovery is compromised, as expected (see Figure 5C), after inhibition of D-NHEJ by treatment

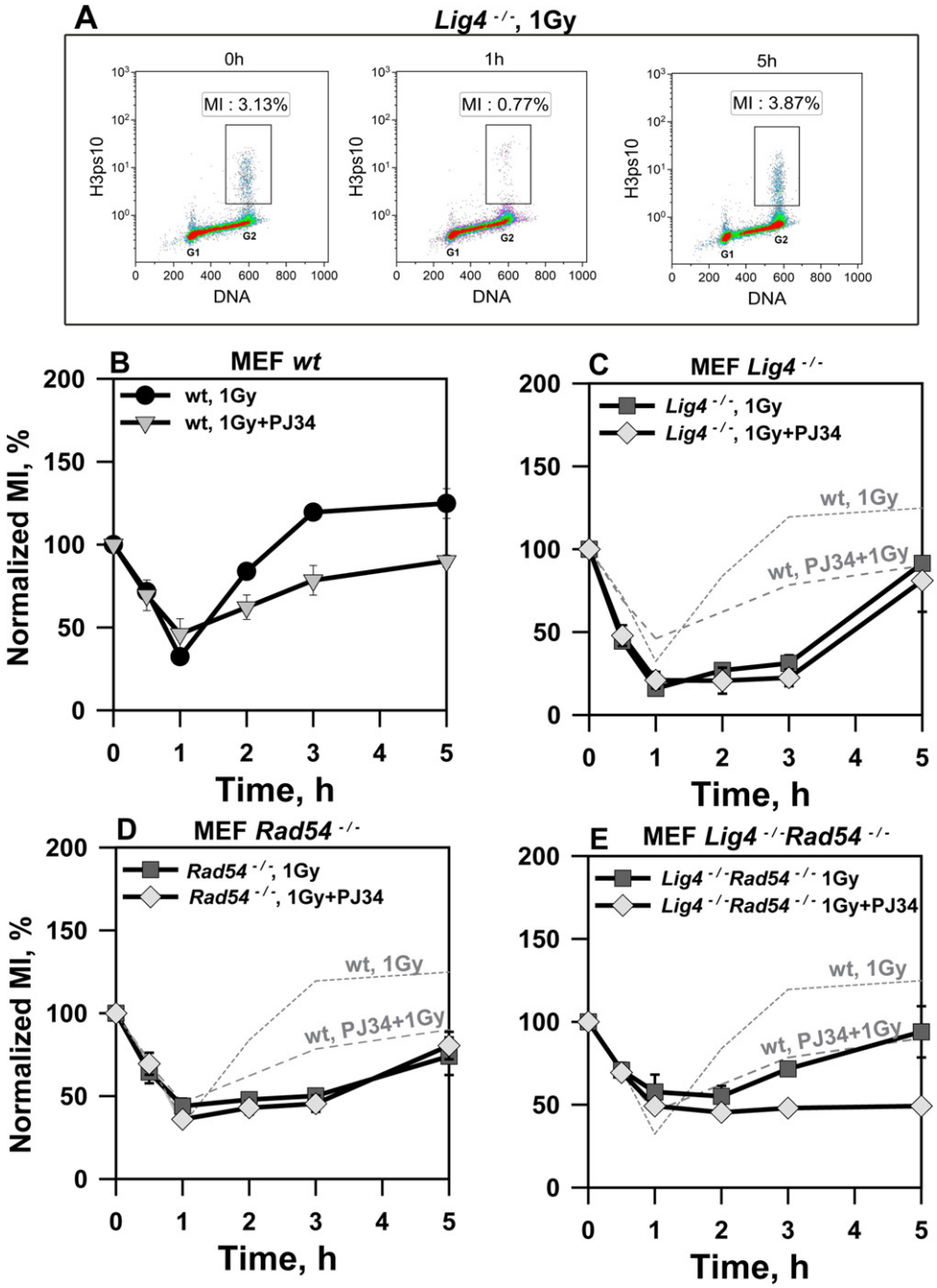

Figure 5. **(A)** Representative two-parametric flow cytometry dot plots of *Lig4*$^{-/-}$ MEFs showing the activation of the G2-checkpoint by determining the MI, defined as the percent of cells at mitosis, through measurement of the fraction H3pS10 positive cells at 0, 1 and 5 h after exposure to 1 Gy IR. The *x*-axis shows the DNA signal measured by PI staining and the *y*-axis the intensity of the H3pS10 signal. Signal within the gates shown indicates that the corresponding cell entered mitosis. **(B)** Effect of Parp inhibition on G2-checkpoint response in wt MEFs after exposure to 1 Gy IR. **(C)** Effect of Parp inhibition on G2-checkpoint in *Lig4*$^{-/-}$ MEFs. Other details as in (B). The dotted and broken lines trace the results of wt cells and have been transferred from panel B. **(D)** As in (C) for *Rad54*$^{-/-}$ MEFs. **(E)** As in (C) for *Lig4*$^{-/-}$*Rad54*$^{-/-}$ MEFs. Data represent the mean ± SD from three to four independent experiments. Where not visible, error bars are smaller than the symbols.

with NU7441. Notably, a similar effect is also observed after inhibition of Lig1 and Lig3 by L67. Since D-NHEJ remains active under these conditions, the observed effect must reflect prolongation of G2-arrest as a result of inhibition of HRR and/or B-NHEJ. Inhibition of D-NHEJ by the combined treatment with NU7441 and L67 completely abrogates recovery of cell division at 4 h after IR (Figure 6A).

Since L67 affects both Lig1 and Lig3, we tested *Lig1*$^{-/-}$ MEFs in an effort to separate the effects of the two ligases. The results obtained are summarized in Figure 6B. In wt MEFs exposed to 1 Gy the MI recovers to control levels 4

h later. Treatment with NU7441 delays as expected this recovery. On the other hand, in *Lig1*$^{-/-}$ MEFs no recovery is observed 4 h after IR. Indeed, the results are highly reminiscent to those obtained in CHO cells after treatment with L67. We infer, therefore, that the main function of L67 in CHO cells is to suppress the function of Lig1 and to compromise in this way HRR. Indeed, the effect observed here is also similar to that measured in *Rad54*$^{-/-}$ MEFs (see Figure 5D). Treatment with NU7441 prevents recovery, again linking B-NHEJ function to the G2-checkpoint recovery. Thus, similarly to HRR and D-NHEJ, also B-NHEJ function is required for a cell to effectively recover from the G2-checkpoint. The intriguing observation for a Lig1 contribution to HRR requires confirmation and further mechanistic analysis.

To better understand the mechanism of B-NHEJ-mediated translocation formation, we studied DNA end resection, specifically in G2 cells, and correlated this endpoint also to the level of activation of the G2-checkpoint. For these experiments we selected *Lig4*$^{-/-}$*Rad54*$^{-/-}$ MEFs, first, because here only B-NHEJ is active in G2-phase, and, second, because they show the highest induction of chromosome translocations 4 h after exposure to 1 Gy IR. This mutant was also interesting because it shows potentiation of the G2-checkpoint after inhibition of Parp with PJ34 (Figure 5E). Figure 6C shows that in this mutant extensive resection takes place in G2 as compared to wt MEFs after exposure to 10 Gy IR. This resection requires MRE11 (51) and is significantly inhibited after treatment with Mirin (Figure 6C). Notably, treatment with Mirin also produces a strong reduction in translocation formation (Figure 6D). This inhibition is further enhanced following combined treatment with Mirin and PJ34. The extensive resection observed in *Lig4*$^{-/-}$*Rad54*$^{-/-}$ MEFs anticipates (Figure 6C) ataxiatelangiectasia and Rad3-related protein (ATR) hyperactivation and explains the strong G2-checkpoint observed in this mutant (Figure 5D).

Collectively, the results of this set of experiments connect B-NHEJ function to DNA end resection, which in turn feeds into the G2-checkpoint possibly through ATR activation. We conclude that DNA end resection provokes translocation formation by B-NHEJ and speculate that the associated enhancement in the checkpoint provides the time needed for 'unrelated' ends to translocate.

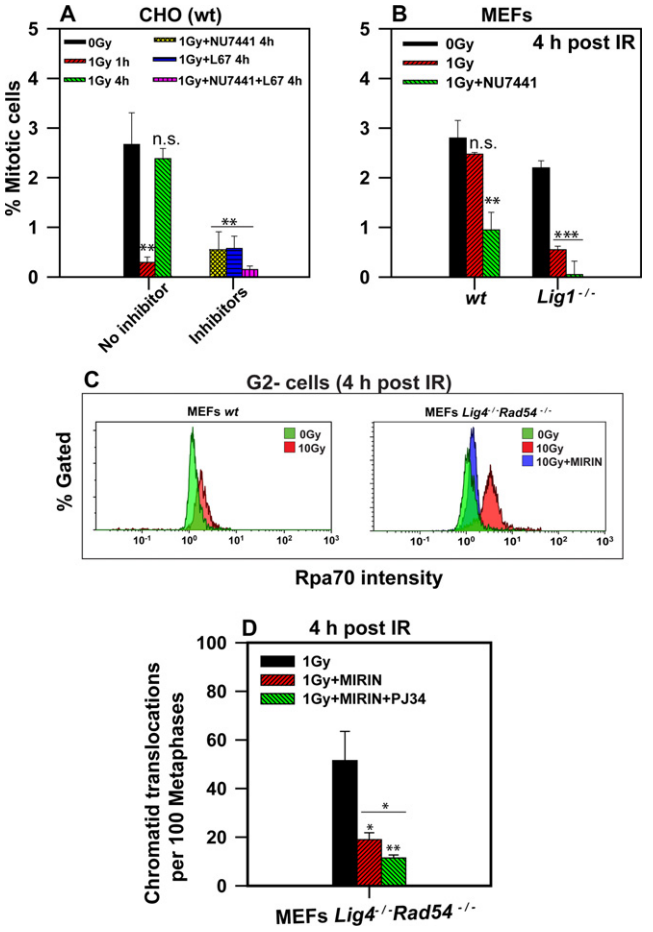

Figure 6. **(A)** G2-checkpoint response in CHO (wt) and EM9 (Xrcc1m) cells exposed to 1 Gy IR with or without NU7441 and/or L67 treatment. The percentage of mitotic cells was determined by counting about 1500–2000 Giemsa-stained cells per sample using bright field microscopy. **(B)** G2-checkpoint response in wt and *Lig1*$^{-/-}$ MEFs exposed to 1 Gy IR alone or in combination with NU7441. **(C)** G2 overlays for Rpa70 intensity showing chromatin bound Rpa in wt and *Lig4*$^{-/-}$*Rad54*$^{-/-}$ MEFs 4 h after exposure to 10 Gy IR. The effect of Mre11 inhibition by Mirin on DSB end resection in *Lig4*$^{-/-}$*Rad54*$^{-/-}$ MEFs is also shown. Fraction of G2 cells was assessed by their DNA content and gated using Kaluza 1.2 software to obtain G2 overlays depicting Rpa intensity. **(D)** Effect of Mirin on the translocation formation in *Lig4*$^{-/-}$*Rad54*$^{-/-}$ MEFs. Results of a Mirin and PJ34 combination is also shown. Data represent the mean ± SD from two to three independent experiments.

DISCUSSION

Alternative end joining is instrumental to translocation formation

Evidence accumulates that alternative end joining plays a dominant role in the formation of chromosome translocations causing cancer or cell lethality (1–2,9,52–54). Alternative end joining causes translocations initiated by RE-generated, site-specific DSBs (26–27,32) but the factors required for this process remain only partly characterized. The results presented here suggest that Parp-1 is an important factor in translocation formation in cells exposed to low IR doses during the G2-phase of the cell cycle where HRR is active and demonstrate that Parp-1 has a substantially stronger contribution of translocation formation than to CB repair. A contribution of Parp-1 to IR-induced translocation formation could also be demonstrated for cells irradiated in G1 phase.

The frequency of translocations in G2 is higher in HRR- or D-NHEJ-deficient cells as compared to the wt and their formation is partly Parp-1 dependent. This suggests the function of B-NHEJ in their formation and implies that in G2, B-NHEJ is backing up not only abrogated D-NHEJ but also abrogated HRR events. Such hierarchical interconnections between DSB repair pathways raise the possibility that even translocations forming in wt cells reflect abrogated D-NHEJ and/or HRR events that are rescued by B-NHEJ. Formal demonstration of this possibility will advance our understanding and also our potential for interception in events known to cause cancer.

The potential of B-NHEJ to backup abrogated HRR also explains the long-held view that alternative pathways of NHEJ utilize (or even require) microhomology (55). Indeed, even if HRR fails at its earliest steps, it is likely that DNA end resection at variable levels will generate single-stranded regions at the ends and will allow fortuitous microhomologies to stabilize DNA ends for the ensuing end joining event. Importantly, however, in this sequence of events, resection and the availability of single-stranded DNA at the ends will be a remnant of the abrogated HRR and not an integral component of B-NHEJ. This observation explains why several essential components of HRR, such as Nbs1 (56), Mre11 (16–18), CtIP (19), etc., have been implicated in B-NHEJ (57), and why B-NHEJ is enhanced in G2-phase (33,34). Finally, the observation that translocation junctions frequently display microhomologies (58,59) may indeed suggest that their formation reflects abrogated HRR events.

Parp-1 is a key contributor to translocation formation, but not necessarily to all DSB repair by alternative end joining

An important finding of the work presented here is that Parp-1 is required for the formation of translocations to a much greater degree than for the mere joining of CBs, or of DSBs. This difference is intriguing because it suggests that it will be possible to develop strategies for suppressing the formation of highly toxic genomic rearrangements without grossly affecting global DSB repair by B-NHEJ. The rapid development of highly specific Parp-1 inhibitors for cancer therapy using the synthetic lethality approach is particularly relevant in this regard (60,61). Indeed, it may prove particularly instructive to integrate the peculiarities of Parp-1 inhibition on B-NHEJ as demonstrated here to the overall synthetic lethality scheme.

We have shown previously that Parp-1 and Ku compete for DNA ends (29). Other work shows that Ku is a critical factor in the regulation of DSB repair pathway choice (50). Here, we demonstrate that the frequency of translocations is increased in the absence of this factor. Indeed, *Ku80*$^{-/-}$ cells show higher incidence of translocations when compared to *DNA-PKcs*$^{-/-}$ and *Lig4*$^{-/-}$ cells, and these events remain sensitive to Parp1 inhibition. This observation further supports the involvement of Parp-1 in translocation formation and emphasizes once more the competitive role played by Ku—even when functioning outside the intact D-NHEJ machinery.

Lig1 and Lig3 contribute to translocation formation; Xrcc1 gives a competitive advantage to Lig3 without being required for its function in translocation formation

The results presented here further implicate Lig1 and Lig3 to the formation of translocations. This extends and complements previous work (see Introduction). The involvement of Lig3 in translocation formation immediately implicates the entire Parp-1/Xrcc1/Lig3 complex in DSB processing. The contributions of Parp-1 have been discussed above. The possible contribution of Xrcc1 is more controversial as some reports implicate this protein in alternative end joining (10,62), while others fail to show such dependence (28,63). Our results with Xrcc1 mutants also show that Xrcc1 is not required for translocation formation. However, our results suggest that while both Lig1 and Lig3 can catalyze the ligation events underlying translocation formation, Lig3 has a strong competitive advantage against Lig1 only in the presence of Xrcc1.

Notably, even in the absence of Xrcc1, translocation formation remains partly sensitive to Parp inhibition suggesting that in this function integration of Parp-1 and Lig3 activities through interaction with Xrcc1 is not required. Furthermore, Parp-1 is clearly required for translocation formation, even in the presence of Lig1, and Parp-1 inhibition by PJ34 severely compromises translocation formation in EM9 cells. It is, therefore, likely that under these conditions, Parp1, and possibly also Lig3, function in a manner that deviates from their canonical operation in the Parp-1/Xrcc1/Lig3 complex.

Activation of the G2-checkpoint by DSBs processed by B-NHEJ: connections with DNA end resection

Here, we also demonstrate for the first time that similarly to HRR and D-NHEJ, also B-NHEJ function is required for a cell to effectively recover from the G2-checkpoint. Indeed, Parp-1 inhibition potentiates the IR-induced G2-checkpoint in wt and the *Lig4*$^{-/-}$*Rad54*$^{-/-}$ MEFs and similar results are obtained by inhibiting DNA ligases 1 and 3. Furthermore, our results link B-NHEJ function to DNA end resection, which in turn can feed into the G2-checkpoint possibly through ATR activation. Collectively, these results suggest that DNA end resection provokes translocation formation by B-NHEJ. Indeed, the associated enhancement in the G2-checkpoint may then provide the time needed for 'unrelated' ends to translocate and join.

CONCLUSIONS

The work presented here demonstrates a critical role for the B-NHEJ components Parp-1, Lig1 and Lig3 in translocation formation from DSBs generated during the G2-phase of the cell cycle and indicates differences in the enzymatic requirements for miss-joining events and normal end joining events during DSB processing by B-NHEJ. Our work also extends the function of B-NHEJ to include backup of abrogated HRR events and provides explanation for the resection occasionally associated with alternative end joining, its apparent requirement for HRR factors, its occasional use of microhomologies and its enhancement during the G2-phase of the cell cycle.

SUPPLEMENTARY DATA

Supplementary Data are available at NAR Online.

ACKNOWLEDGMENTS

We would like to thank Drs. Frederick W. Alt, Eric A. Hendrickson, David Melton, John Thacker and Zhao-Qi Wang for providing cell lines. We would also like to thank Tamara Muβfeldt for excellent technical support.

FUNDING

Deutsche Forschungsgemeinschaft (DFG) Graduate training program [GRK1431]; BMBF and BMWi. Source of Open Access funding: University Funding for the Institute.1. Funding for open access charge: DFG [GRK 1431].
Conflict of interest statement. None declared.

REFERENCES

1. Roukos,V., Voss,T.C., Schmidt,C.K., Lee,S., Wangsa,D. and Misteli,T. (2013) Spatial dynamics of chromosome translocations in living cells. *Science*, **341**, 660–664.
2. Bunting,S.F. and Nussenzweig,A. (2013) End-joining, translocations and cancer. *Nat. Rev. Cancer*, **13**, 443–454.
3. Loucas,B.D. and Cornforth,M.N. (2013) The LET dependence of unrepaired chromosome damage in human cells: a break too far? *Radiat. Res.*, **179**, 393–405.
4. Lieber,M.R. (2010) The mechanism of double-strand DNA break repair by the nonhomologous DNA end-joining pathway. *Annu. Rev. Biochem.*, **79**, 1.1–1.31.
5. Mladenov,E. and Iliakis,G. (2011) Induction and repair of DNA double strand breaks: the increasing spectrum of non-homologous end joining pathways. *Mut. Res./Fundamental Mol. Mech. Mutagen.*, **711**, 61–72.
6. Kinner,A., Wu,W., Staudt,C. and Iliakis,G. (2008) γ-H2AX in recognition and signaling of DNA double-strand breaks in the context of chromatin. *Nucleic Acids Res.*, **36**, 5678–5694.
7. San Filippo,J., Sung,P. and Klein,H. (2008) Mechanism of eukaryotic homologous recombination. *Annu. Rev. Biochem.*, **77**, 229–257.
8. Iliakis,G. (2009) Backup pathways of NHEJ in cells of higher eukaryotes: cell cycle dependence. *Radiother. Oncol.*, **92**, 310–315.
9. Schipler,A. and Iliakis,G. (2013) DNA double-strand-break complexity levels and their possible contributions to the probability for error-prone processing and repair pathway choice. *Nucleic Acids Res.*, **41**, 7589–7605.
10. Audebert,M., Salles,B. and Calsou,P. (2004) Involvement of poly(ADP-ribose) polymerase-1 and XRCC1/DNA ligase III in an alternative route for DNA double-strand breaks rejoining. *J. Biol. Chem.*, **279**, 55117–55126.
11. Wang,H., Rosidi,B., Perrault,R., Wang,M., Zhang,L., Windhofer,F. and Iliakis,G. (2005) DNA ligase III as a candidate component of backup pathways of nonhomologous end joining. *Cancer Res.*, **65**, 4020–4030.
12. Mansour,W.Y., Rhein,T. and Dahm-Daphi,J. (2010) The alternative end-joining pathway for repair of DNA double-strand breaks requires PARP1 but is not dependent upon microhomologies. *Nucleic Acids Res.*, **38**, 6065–6077.
13. Liang,L., Deng,L., Nguyen,S.C., Zhao,X., Maulion,C.D., Shao,C. and Tischfield,J.A. (2008) Human DNA ligases I and III, but not ligase IV, are required for microhomology-mediated end joining of DNA double-strand breaks. *Nucleic Acids Res.*, **36**, 3297–3310.
14. Arakawa,H., Bednar,T., Wang,M., Paul,K., Mladenov,E., Bencsik-Theilen,A.A. and Iliakis,G. (2012) Functional redundancy between DNA ligases I and III in DNA replication in vertebrate cells. *Nucleic Acids Res.*, **40**, 2599–2610.
15. Paul,K., Wang,M., Mladenov,E., Bencsik-Theilen,A.A., Bednar,T., Wu,W., Arakawa,H. and Iliakis,G. (2013) DNA ligases I and III cooperate in alternative non-homologous end-joining in vertebrates. *PLoS One*, **8**, e59505.
16. Rass,E., Grabarz,A., Plo,I., Gautier,J., Bertrand,P. and Lopez,B.S. (2009) Role of Mre11 in chromosomal nonhomologous end joining in mammalian cells. *Nat. Struct. Mol. Biol.*, **16**, 819–825.
17. Dinkelmann,M., Spehalski,E., Stoneham,T., Buis,J., Wu,Y., Sekiguchi,J.M. and Ferguson,D.O. (2009) Multiple functions of MRN in end-joining pathways during isotype class switching. *Nat. Struct. Mol. Biol.*, **16**, 808–813.
18. Xie,A., Kwok,A. and Scully,R. (2009) Role of mammalian Mre11 in classical and alternative nonhomologous end joining. *Nat. Struct. Mol. Biol.*, **16**, 814–818.
19. Zhang,Y. and Jasin,M. (2011) An essential role for CtIP in chromosomal translocation formation through an alternative end-joining pathway. *Nat. Struct. Mol. Biol.*, **18**, 80–84.
20. Zhang,Y. and Rowley,J.D. (2006) Chromatin structural elements and chromosomal translocations in leukemia. *DNA Repair*, **5**, 1282–1297.
21. Kelly,L.M. and Gilliland,D.G. (2002) Genetics of myeloid leukemias. *Annu. Rev. Genom. Hum. Genet.*, **3**, 179–198.
22. Nickoloff,J.A., De Haro,L.P., Wray,J. and Hromas,R. (2008) Mechanisms of leukemia translocations. *Curr. Opin. Hematol.*, **15**, 338–345.
23. Ferguson,D.O., Sekiguchi,J.M., Chang,S., Frank,K.M., Gao,Y., DePinho,R.A. and Alt,F.W. (2000) The nonhomologous end-joining pathway of DNA repair is required for genomic stability and the suppression of translocations. *Proc. Natl. Acad. Sci. U.S.A.*, **97**, 6630–6633.
24. Weinstock,D.M., Brunet,E. and Jasin,M. (2007) Formation of NHEJ-derived reciprocal chromosomal translocations does not require Ku70. *Nat. Cell Biol.*, **9**, 978–981.
25. Simsek,D. and Jasin,M. (2010) Alternative end-joining is suppressed by the canonical NHEJ component Xrcc4-ligase IV during chromosomal translocation formation. *Nat. Struct. Mol. Biol.*, **17**, 410–416.
26. Simsek,D., Brunet,E., Wong,S.Y.-W., Katyal,S., Gao,Y., McKinnon,P.J., Lou,J., Zhang,L., Li,J., Rebar,E.J. *et al.* (2011) DNA ligase III promotes alternative nonhomologous end-joining during chromosomal translocation formation. *PLoS Genet.*, **7**, e1002080.
27. Combs,S.E. and Debus,J. (2013) Treatment with heavy charged particles: systematic review of clinical data and current clinical (comparative) trials. *Acta Oncol.*, **52**, 1272–1286.
28. Boboila,C., Oksenych,V., Gostissa,M., Wang,J.H., Zha,S., Zhang,Y., Chai,H., Lee,C.-S., Jankovic,M., Saez,L.-M.A. *et al.* (2012) Robust chromosomal DNA repair via alternative end-joining in the absence of X-ray repair cross-complementing protein 1 (XRCC1). *Proc. Natl. Acad. Sci. U.S.A.*, **109**, 2473–2478.
29. Wang,M., Wu,W., Wu,W., Rosidi,B., Zhang,L., Wang,H. and Iliakis,G. (2006) PARP-1 and Ku compete for repair of DNA double strand breaks by distinct NHEJ pathways. *Nucleic Acids Res.*, **34**, 6170–6182.
30. Bryant,H.E., Schultz,N., Thomas,H.D., Parker,K.M., Flower,D., Lopez,E., Kyle,S., Meuth,M., Curtin,N.J. and Helleday,T. (2005) Specific killing of BRCA2-deficient tumours with inhibitors of poly(ADP-ribose) polymerase. *Nature*, **434**, 913–917.
31. Farmer,H., McCabe,N., Lord,C.J., Tutt,A.N.J., Johnson,D.A., Richardson,T.B., Santarosa,M., Dillon,K.J., Hickson,I., Knights,C. *et al.* (2005) Targeting the DNA repair defect in BRCA mutant cells as a therapeutic strategy. *Nature*, **434**, 917–921.
32. Wray,J., Williamson,E.A., Singh,S.B., Wu,Y., Cogle,C.R., Weinstock,D.M., Zhang,Y., Lee,S.-H., Zhou,D., Shao,L. *et al.* (2013) PARP1 is required for chromosomal translocations. *Blood*, **121**, 4359–4365.
33. Wu,W., Wang,M., Wu,W., Singh,S.K., Mussfeldt,T. and Iliakis,G. (2008) Repair of radiation induced DNA double strand breaks by backup NHEJ is enhanced in G2. *DNA Repair*, **7**, 329–338.
34. Wu,W., Wang,M., Mussfeldt,T. and Iliakis,G. (2008) Enhanced use of backup pathways of NHEJ in G_2 in Chinese hamster mutant cells with defects in the classical pathway of NHEJ. *Radiat. Res.*, **170**, 512–520.
35. Yang,Y.-G., Cortes,U., Patnaik,S., Jasin,M. and Wang,Z.-Q. (2004) Ablation of PARP-1 does not interfere with the repair of DNA double-strand breaks, but compromises the reactivation of stalled replication forks. *Oncogene*, **23**, 3872–3882.
36. Chen,X., Zhong,S., Zhu,X., Dziegielewska,B., Ellenberger,T., Wilson,G.M., MacKerell,A.D. Jr and Tomkinson,A.E. (2008) Rational design of human DNA ligase inhibitors that target cellular DNA replication and repair. *Cancer Res.*, **68**, 3169–3177.
37. Bryant,P.E., Mozdarani,H. and Marr,C. (2008) G2-phase chromatid break kinetics in irradiated DNA repair mutant hamster cell lines using calyculin-induced PCC and colcemid-block. *Mutat. Res.*, **657**, 8–12.
38. V Forment,Josep, V Walker,Rachael and P Jackson,Stephen (2012) A high-throughput, flow cytometry-based method to quantify DNA-end resection in mammalian cells. *Cytometry. Part A : the journal of the International Society for Analytical Cytology*, **81**, 922–928. [PubMed]
39. Bryant,P.E. and Mozdarani,H. (2007) A comparison of G2 phase radiation-induced chromatid break kinetics using calyculin-PCC with those obtained using colcemid block. *Mutagenesis*, **22**, 359–362.

40. Shovman,O., Riches,A.C., Adamson,D. and Bryant,P.E. (2008) An improved assay for radiation-induced chromatid breaks using a colcemid block and calyculin-induced PCC combination. *Mutagenesis*, **23**, 267–270.
41. Terry,S.Y.A., Riches,A.C. and Bryant,P.E. (2009) Suppression of topoisomerase IIα expression and function in human cells decreases chromosomal radiosensitivity. *Mut. Res./Fundamental Mol. Mech. Mutagen.*, **663**, 40–45.
42. Bryant,P.E., Riches,A.C. and Terry,S.Y.A. (2010) Mechanisms of the formation of radiation-induced chromosomal aberrations. *Mut. Res./Genet. Toxicol. Environment. Mutagen.*, **701**, 23–26.
43. Bryant,P.E., Riches,A.C., Shovman,O., Dewar,J.A. and Adamson,D.J.A. (2012) Topoisomerase IIα levels and G2 radiosensitivity in T-lymphocytes of women presenting with breast cancer. *Mutagenesis*, **27**, 737–741.
44. DiBiase,S.J., Zeng,Z.-C., Chen,R., Hyslop,T., Curran,W.J. Jr and Iliakis,G. (2000) DNA-dependent protein kinase stimulates an independently active, nonhomologous, end-joining apparatus. *Cancer Res.*, **60**, 1245–1253.
45. Singh,S.K., Wu,W., Wu,W., Wang,M. and Iliakis,G. (2009) Extensive repair of DNA double-strand breaks in cells deficient in the DNA-PK dependent pathway of NHEJ after exclusion of heat-labile sites. *Radiat. Res.*, **172**, 152–164.
46. Iliakis,G., Wang,H., Perrault,A.R., Boecker,W., Rosidi,B., Windhofer,F., Wu,W., Guan,J., Terzoudi,G. and Pantelias,G. (2004) Mechanisms of DNA double strand break repair and chromosome aberration formation. *Cytogenet. Genome. Res.*, **104**, 14–20.
47. Robert,I., Dantzer,F. and Reina-San-Martin,B. (2009) Parp1 facilitates alternative NHEJ, whereas Parp2 suppresses IgH/c-myc translocations during immunoglobulin class switch recombination. *J. Exp. Med.*, **206**, 1047–1056.
48. Abdelkarim,G.E., Gertz,K., Harms,C., Katchanov,J., Dirnagl,U., Szabo,C. and Endres,M. (2001) Protective effects of PJ34, a novel, potent inhibitor of poly(ADP-ribose) polymerase (PARP) in in vitro and in vivo models of stroke. *Int. J. Mol. Med.*, **7**, 255–260.
49. Garcia Soriano,F., Virag,L., Jagtap,P., Szabo,E., Mabley,J.G., Liaudet,L., Marton,A., Hoyt,D.G., Murthy,K.G.K., Salzman,A.L. *et al.* (2001) Diabetic endothelial dysfunction: the role of poly(ADP-ribose) polymerase activation. *Nat. Med.*, **7**, 108–113.
50. Fattah,F., Lee,E.H., Weisensel,N., Wang,Y., Lichter,N. and Hendrickson,E.A. (2010) Ku regulates the non-homologous end joining pathway choice of DNA double-strand break repair in human somatic cells. *PLoS Genet.*, **6**, e1000855.
51. Shibata,A., Moiani,D., Arvai,A.S., Perry,J., Harding,S.M., Genois,M.-M., Maity,R., van Rossum-Fikkert,S., Kertokalio,A., Romoli,F. *et al.* (2014) DNA double-strand break repair pathway choice is directed by distinct MRE11 nuclease activities. *Mol. Cell*, **53**, 7–18.
52. Iliakis,G., Wu,W., Wang,M., Terzoudi,G.I. and Pantelias,G.E. (2007) Backup Pathways of Nonhomologous End joining May Have a Dominant Role in the Formation of Chromosome Aberrations. In: Obe,G. and Vijayalaxmi, (eds).,*Chromosomal Alterations*. Springer Verlag, Berlin, Heidelberg, New York, pp. 67–85.
53. Boboila,C., Alt,F.W. and Schwer,B. (2012) In Frederick,W.A. (ed.), *Advances in Immunology*, Vol. 116. Academic Press, pp. 1–49.
54. Alt,Frederick W., Zhang,Y., Meng,F.-L., Guo,C. and Schwer,B. (2013) Mechanisms of programmed DNA lesions and genomic instability in the immune system. *Cell*, **152**, 417–429.
55. McVey,M. and Lee,S.E. (2008) MMEJ repair of double-strand breaks (director's cut): deleted sequences and alternative endings. *Trends Genet.*, **24**, 529–538.
56. Deriano,L., Stracker,T.H., Baker,A., Petrini,J.H.J. and Roth,D.B. (2009) Roles for NBS1 in alternative nonhomologous end-joining of V(D)J recombination intermediates. *Mol. Cell*, **34**, 13–25.
57. Truong,L.N., Li,Y., Shi,L.Z., Hwang,P.Y.-H., He,J., Wang,H., Razavian,N., Berns,M.W. and Wu,X. (2013) Microhomology-mediated end joining and homologus recombination share the initial end resection step to repair DNA double-strand breaks in mammalian cells. *Proc. Natl. Acad. Sci. U.S.A.*, **110**, 7720–7725.
58. Zhu,C., Mills,K.D., Ferguson,D.O., Lee,C., Manis,J., Fleming,J., Gao,Y., Morton,C.C. and Alt,F.W. (2002) Unrepaired DNA breaks in p53-deficient cells lead to oncogenic gene amplification subsequent to translocations. *Cell*, **109**, 811–821.
59. Weinstock,D.M., Elliott,B. and Jasin,M. (2006) A model of oncogenic rearrangements: differences between chromosomal translocation mechanisms and simple double-strand break repair. *Blood*, **107**, 777–780.
60. Lord,C.J. and Ashworth,A. (2013) Mechanisms of resistance to therapies targeting BRCA-mutant cancers. *Nat. Med.*, **19**, 1381–1388.
61. Lord,C.J. and Ashworth,A. (2012) The DNA damage response and cancer therapy. *Nature*, **481**, 287–294.
62. Saribasak,H., Maul,R.W., Cao,Z., McClure,R.L., Yang,W., McNeill,D.R., Wilson,D.M. and Gearhart,P.J. (2011) XRCC1 suppresses somatic hypermutation and promotes alternative nonhomologous end joining in Igh genes. *J. Exp. Med.*, **208**, 2209–2216.
63. Han,L., Mao,W. and Yu,K. (2012) X-ray repair cross-complementing protein 1 (XRCC1) deficiency enhances class switch recombination and is permissive for alternative end joining. *Proc. Natl. Acad. Sci. U.S.A.*, **109**, 4604–4608.